



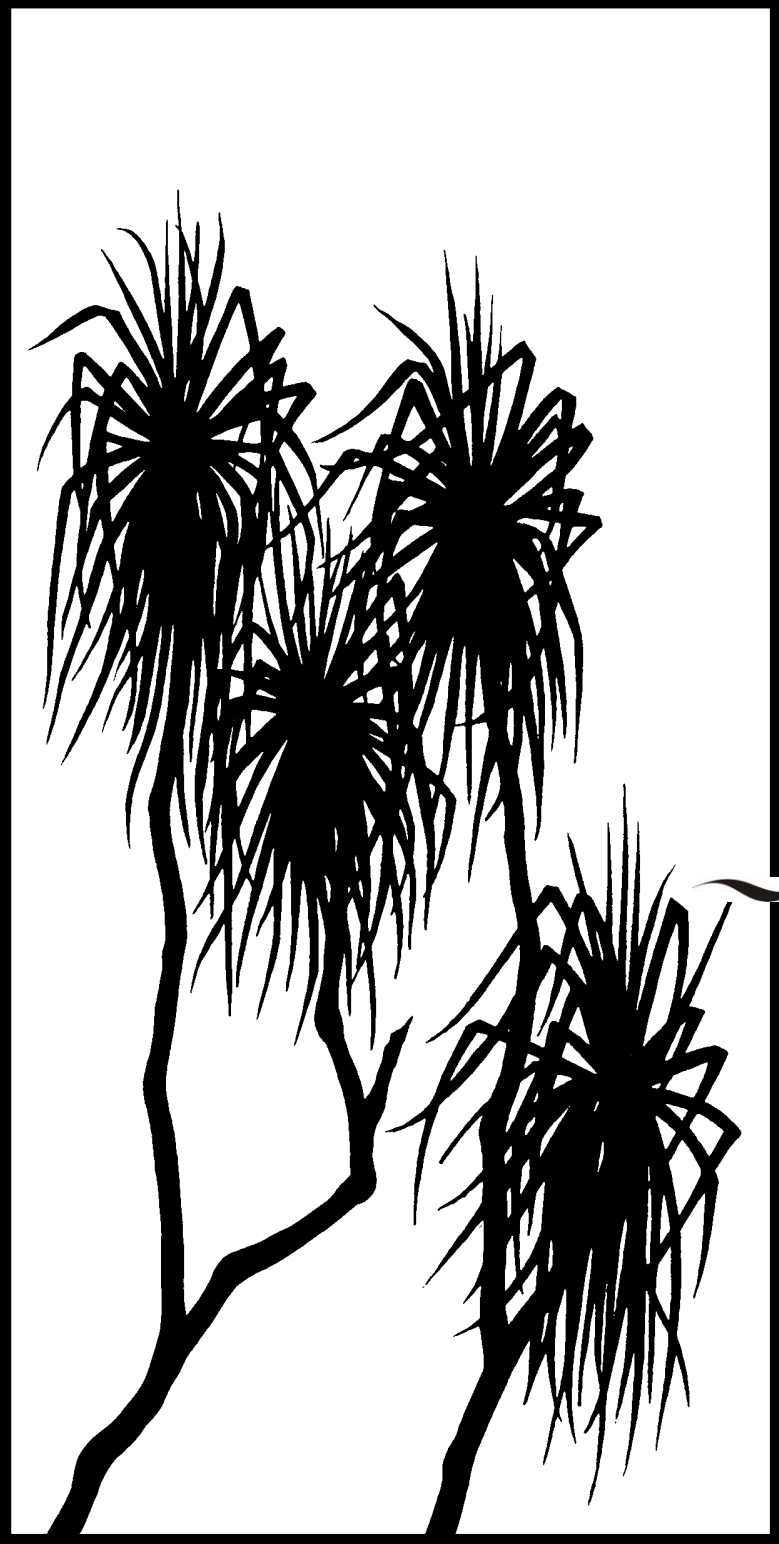
Australian Government

Department of Agriculture, Water and the Environment

Supervising Scientist

*internal  
report*

662

A large black silhouette of several Pandanus trees, showing their characteristic prop roots and dense, spiky foliage, enclosed in a black rectangular frame.

Radon-222 diffusion  
from acrylic containers  
used in eriss gamma  
spectrometry analysis

John Pfitzner & Scott McMaster

June 2021

Release status – Unrestricted

Project number – RES-2019-023

*The Department acknowledges the traditional custodians of country throughout Australia and their continuing connection to land, sea and community. We pay our respects to them and their cultures and to their elders both past and present.*

# Radon-222 diffusion from acrylic containers used in eriss gamma spectrometry analysis

**John Pfitzner & Scott McMaster**

Supervising Scientist  
GPO Box 461, Darwin NT 0801

June 2021

(Release status – Unrestricted)



**Australian Government**

---

**Department of Agriculture, Water and the Environment**

Supervising Scientist

*How to cite this report:*

Pfitzner J & McMaster S 2021. Radon-222 diffusion from acrylic containers used in eriss gamma spectrometry analysis. Internal Report 662, June 2021, Supervising Scientist, Darwin.

*Project number: (RES-2019-023)*

*Authors of this report:*

John Pfizner –Supervising Scientist, GPO Box 461, Darwin NT 0801, Australia

Scott McMaster –Supervising Scientist, GPO Box 461, Darwin NT 0801, Australia

Supervising Scientist is a branch of the Australian Government Department of Agriculture, Water and the Environment.

Supervising Scientist

Department of Agriculture, Water and the Environment

GPO Box 461, Darwin NT 0801 Australia

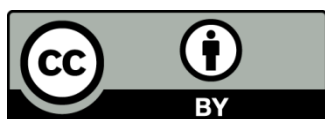
[environment.gov.au/science/supervising-scientist/publications](http://environment.gov.au/science/supervising-scientist/publications)

© Commonwealth of Australia 2021

## Ownership of intellectual property rights

Unless otherwise noted, copyright (and any other intellectual property rights) in this publication is owned by the Commonwealth of Australia (referred to as the Commonwealth).

Creative Commons licence All material in this publication is licensed under a Creative Commons Attribution 4.0 International Licence except content supplied by third parties, logos and the Commonwealth Coat of Arms. Inquiries about the licence and any use of this document should be emailed to [copyright@awe.gov.au](mailto:copyright@awe.gov.au).



The Australian Government acting through the Department of Agriculture, Water and the Environment has exercised due care and skill in preparing and compiling the information and data in this publication. Notwithstanding, the Department of Agriculture, Water and the Environment, its employees and advisers disclaim all liability, including liability for negligence and for any loss, damage, injury, expense or cost incurred by any person as a result of accessing, using or relying on any of the information or data in this publication to the maximum extent permitted by law.

# Contents

<b>Contents</b>	<b>iv</b>
<b>Executive summary</b>	<b>v</b>
<b>1 Introduction</b>	<b>6</b>
1.1 Background	6
1.2 Aim	10
<b>2 Experimental methods</b>	<b>10</b>
2.1 Samples	10
2.2 Test chambers	11
2.3 RAD7 radon detectors	11
2.4 HPGe gamma detectors	12
<b>3 Results and discussion</b>	<b>13</b>
3.1 $^{222}\text{Rn}$ leakage	13
3.2 Free $^{222}\text{Rn}$	16
3.3 Identifying $^{222}\text{Rn}$ leakers	19
<b>4 Conclusion</b>	<b>22</b>
<b>References</b>	<b>23</b>
<b>Appendix A RAD7 cross-calibration plots</b>	<b>24</b>
<b>Appendix B RAD7 measurement data</b>	<b>25</b>

## Executive summary

Radium-226 ( $^{226}\text{Ra}$ ) is a radionuclide of importance in post-mining rehabilitation dose calculations. Gamma spectrometry is used to measure  $^{226}\text{Ra}$  in soils, sediments and biota. The principal gamma emission line for  $^{226}\text{Ra}$  is of low emission intensity and is overlaid with an emission line of uranium-235 ( $^{235}\text{U}$ ). Greater accuracy of  $^{226}\text{Ra}$  activity can be gained by measuring stronger gamma emissions from radionuclides further down the uranium-238 ( $^{238}\text{U}$ ) decay chain. However, this method relies on the retention of the noble gas radon-222 ( $^{222}\text{Rn}$ ) within the sample container, so that its progeny radionuclides, bismuth-214 ( $^{214}\text{Bi}$ ) and lead-214 ( $^{214}\text{Pb}$ ), can reach secular equilibrium with  $^{226}\text{Ra}$ . The acrylic sample containers in use at the Environmental Research Institute of the Supervising Scientist (eriss) have been tested for  $^{222}\text{Rn}$  diffusion to ensure that the reported  $^{226}\text{Ra}$  results are consistently accurate.

In the samples that we tested the diffusion of  $^{222}\text{Rn}$  was consistently low and ranged from 0.74–1.5% of the total  $^{222}\text{Rn}$  (or  $^{226}\text{Ra}$ ) activity in the sample. This diffusion was found to not have a significant effect on reported  $^{226}\text{Ra}$  activity concentrations measured by gamma spectrometry, as calibration and counting uncertainties are typically larger than these  $^{222}\text{Rn}$  losses. Moreover, the  $^{222}\text{Rn}$  diffusion is comparable between detector calibration standards and environmental samples, further reducing any effect on the reported  $^{226}\text{Ra}$  results.

Tests for free  $^{222}\text{Rn}$  (i.e.  $^{222}\text{Rn}$  that has emanated from the sample material and is potentially free to escape the acrylic container if not properly sealed) were also conducted. The tests showed that a considerable percentage (>50% for some sample matrices) of the  $^{222}\text{Rn}$  in the containers is free, highlighting the need to carefully follow the existing procedure for gamma spectrometry sample preparation to avoid any excessive loss of  $^{222}\text{Rn}$ , identified here as 'leakage'. This will ensure that high standards of accuracy and precision are maintained in measuring and reporting  $^{226}\text{Ra}$  activity concentrations in environmental samples analysed by gamma spectrometry.

If the seal between the acrylic container, lid and o-ring are not radon tight, leakage of  $^{222}\text{Rn}$  will be apparent in the gamma spectrometry results, where the  $^{226}\text{Ra}$  calculated from  $^{214}\text{Bi}$  and  $^{214}\text{Pb}$  will appear to be lower activity than the  $^{226}\text{Ra}$  measured directly at 186.2 keV. In these rare cases, the cause is often excessive sample which prevents the lid, o-ring and container contacting with sufficient pressure. This is remedied by the removal of excess sample material, with the appropriate adjustment to the weight used in calculations, and requires repacking, careful resealing and then recounting after reaching secular equilibrium.

# 1 Introduction

## 1.1 Background

The Environmental Research Institute of the Supervising Scientist (eriss) uses gamma spectrometry to measure radionuclides in a range of environmental samples including milled rock, sediments, soils and biota (Murray et al 1987). Radium-226 ( $^{226}\text{Ra}$ ) is a radionuclide of particular interest due to its potential to contribute a radiation dose to the public, particularly via consumption of freshwater mussels (Bollhöfer et al 2011) and as the precursor of radioactive radon-222 ( $^{222}\text{Rn}$ ) gas (Doering et al 2018).

Gamma spectrometry measurement of  $^{226}\text{Ra}$  can be performed directly using the 186.2 keV emission line, although its relatively low emission intensity (3.6%) (LNHB 2021) and conflict with a similar emission energy of uranium-235 ( $^{235}\text{U}$ ) at 185.7 keV can result in high uncertainties. To overcome this,  $^{226}\text{Ra}$  activity is determined based on the measurement of higher emission intensity radionuclides further down the uranium-238 ( $^{238}\text{U}$ ) decay chain. These radionuclides are bismuth-214 ( $^{214}\text{Bi}$ ) (45.5% intensity @ 609 keV) and lead-214 ( $^{214}\text{Pb}$ ) (35.6% intensity @ 352 keV and 18.4% @ 295 keV) (LNHB 2021). However, this technique relies on the sample measurement container retaining all of the elusive  $^{222}\text{Rn}$  gas, so that secular equilibrium can be reached between  $^{222}\text{Rn}$ ,  $^{214}\text{Bi}$  &  $^{214}\text{Pb}$ , and  $^{226}\text{Ra}$  (Figure 1). To achieve greater than 98% secular equilibrium, samples need to be sealed in air-tight containers and stored until at least six half-lives of  $^{222}\text{Rn}$  (>23 days) have elapsed prior to analysis. Radon-222 leakage from a sample container can cause the reported  $^{226}\text{Ra}$  activity concentration to be underestimated. Conversely,  $^{222}\text{Rn}$  leakage from the measurement container of a detector calibration standard can result in an overestimate of reported  $^{226}\text{Ra}$  activity concentration in samples due to detector efficiency being underestimated.

Historically at eriss, pulverised solid samples and calibration standards had been prepared for gamma spectrometry analysis by casting in polyester resin (Murray 1987, Marten 1992, Pfitzner 1993) (Figure 2). Although the resin casting method gave reliable results, there were specific workplace health and safety (WHS) risks involved with the sample preparation method due to the use of chemical substances. Also, the destructive nature of the resin casting method essentially destroys the sample for any further analysis. Consequently, in 2002, it was decided to change the method of sample preparation for gamma spectrometry.

As no containers with volumes between 5 and 50 cm<sup>3</sup> designed specifically for gamma spectrometry were available, several other laboratories have re-purposed existing containers, including steel and aluminium tins, glass jars and petri dishes, with varying degrees of success (Suursoon et al 2014, Drew Watson Queensland Health pers. comm., Jon Ollie University of Queensland pers. comm.). Steel containers have the problem of attenuation at low gamma energies which particularly affects lead-210 ( $^{210}\text{Pb}$ ) gamma emissions at 46.5 keV. Steel and glass can have varying backgrounds of radionuclide activity which impacts the ability to confidently analyse samples of low activity. Suitable sized steel and aluminium containers are generally not available with hermetic seals, so improvised seals are employed, most commonly epoxy resin (e.g. Araldite). If epoxy resin was used, the sample could only be retrieved by destruction of the container or by using solvents to dissolve the epoxy resin, both methods of sample removal increase the WHS risks and potentially cause sample contamination.

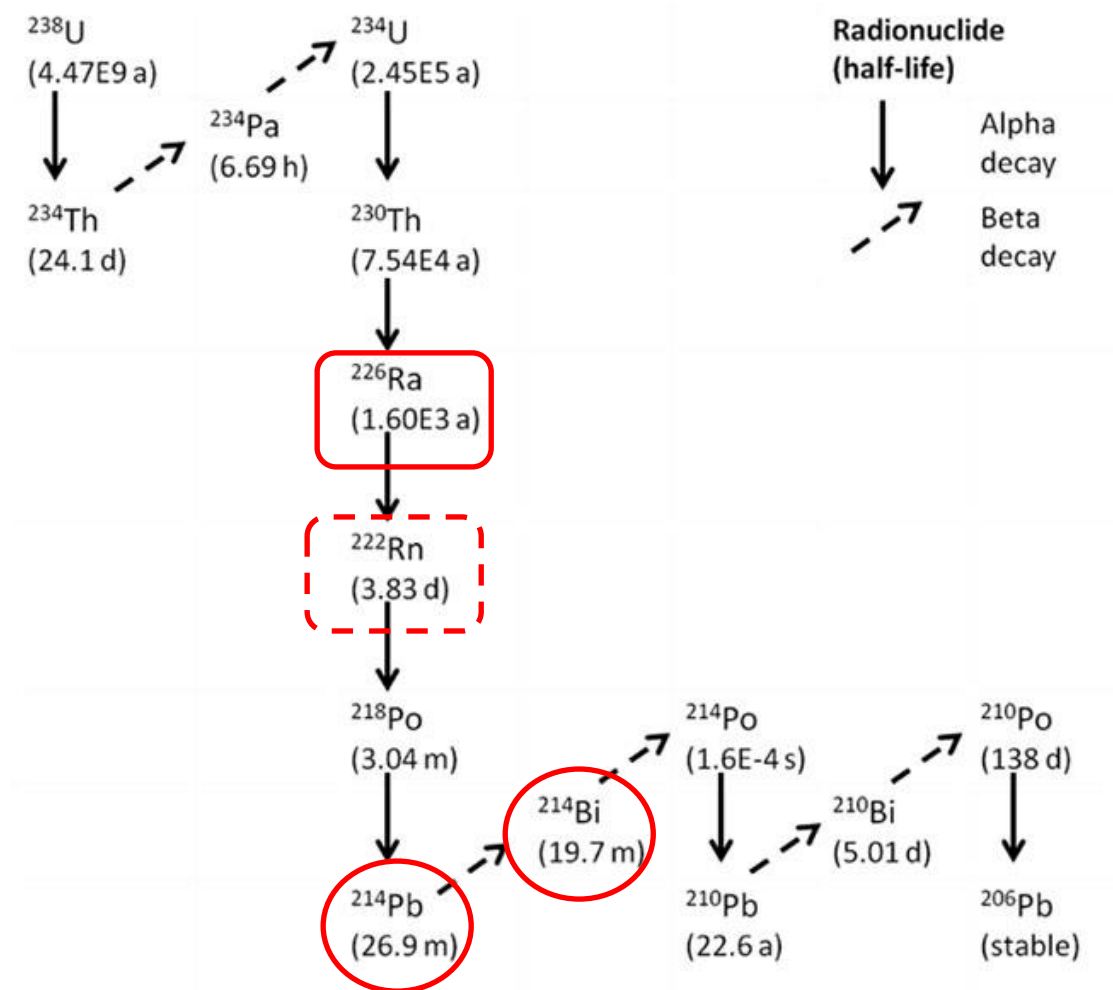


**Figure 1**  $^{238}\text{U}$  decay chain, highlighting the relationship between  $^{226}\text{Ra}$ ,  $^{222}\text{Rn}$  and  $^{214}\text{Bi}$  and  $^{214}\text{Pb}$ .



**Figure 2** Pre-2002 resin style casts for gamma spectrometry analysis.



Eriss opted for resealable acrylic containers which were originally designed and manufactured by the Australian Institute of Marine Science (AIMS) and subsequently produced and adopted by several other gamma spectrometry laboratories. The acrylic containers consist of five components:

1. a machined acrylic base which holds the pressed pulverised sample material and has a groove for an o-ring and a threaded body to match a screw cap;
2. a rubber o-ring;
3. a clear acrylic disc or lid to seal against the o-ring;
4. a screw cap to ensure a tight seal between the base, o-ring and disc lid; and
5. vacuum grease or Vaseline which assists in sealing the o-ring.

A significant additional component of the acrylic container usage by eriss is the hydraulic press (Figure 3) which compresses the powdered sample material into the base, to maximize the quantity of material in the container and for consistent density. The use of the hydraulic press is described in the eriss standard operating procedure for 'Gamma Sample Pressing'.



**Figure 3** Hydraulic press for compressing sample material into acrylic containers.

Three sizes of acrylic containers are currently used by eriss and are shown in Figure 4. The eriss designation of the different container sizes (geometries) and their nominal sample capacities are:

- 'B',  $1.6 \text{ cm}^3$  (20 mm diameter  $\times$  5 mm depth);
- 'Q',  $8 \text{ cm}^3$  (45 mm diameter  $\times$  5 mm depth); and
- 'R',  $92 \text{ cm}^3$  (73 mm diameter  $\times$  22 mm depth).

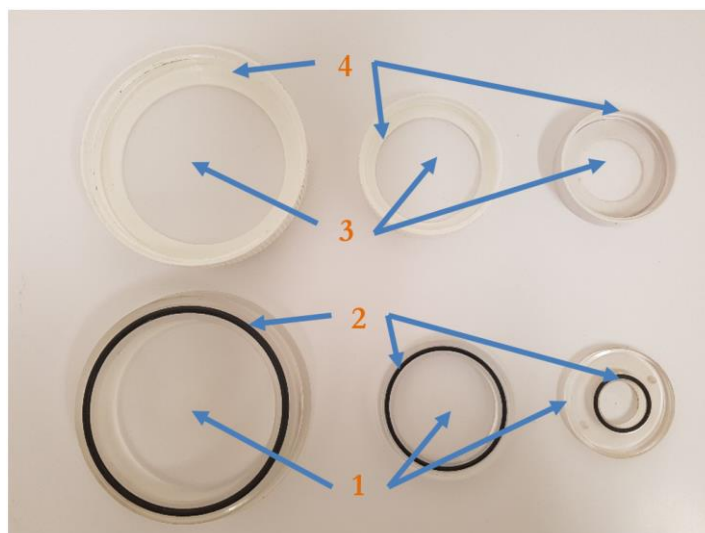


**Figure 4** Eriss acrylic containers of designation R, Q and B (left to right). Numbered components are identified in the text, except for the vacuum grease which is applied to the o-rings.

Gamma spectrometry analysis of samples in these acrylic containers has been a standard practice at eriss for almost 20 years and at AIMS for 11 years (1995–2006). They have also been used at other Australian laboratories including the former Commonwealth Scientific and Industrial Research Organisation (CSIRO) Land and Water laboratories (Leslie 2009) and Australian National University (ANU) (Dr Steve Tims pers. comm.). Using the containers, these laboratories participated in  $^{226}\text{Ra}$  proficiency tests conducted by the International Atomic Energy Agency (IAEA) and other groups, covering a range of radiation measurement activities (IAEA 2010). The  $^{226}\text{Ra}$  activity concentrations reported by the Australian laboratories were within the range of other participating laboratories, indicating that gamma measurement of  $^{214}\text{Bi}$  and  $^{214}\text{Pb}$  was at approximate secular equilibrium with  $^{226}\text{Ra}$  and hence that the leakage of  $^{222}\text{Rn}$  was low.

The designers of the containers were aware of the potential for  $^{222}\text{Rn}$  diffusion through acrylic material. To mitigate this effect, acrylic sheet was used for manufacturing the base such that the extrusion flow, and any imperfections associated with the extrusion process, were across the base, not through the base (Figure 5). All container bases manufactured at AIMS were made from acrylic sheet, not acrylic rods. Lids were also cut from acrylic sheet.

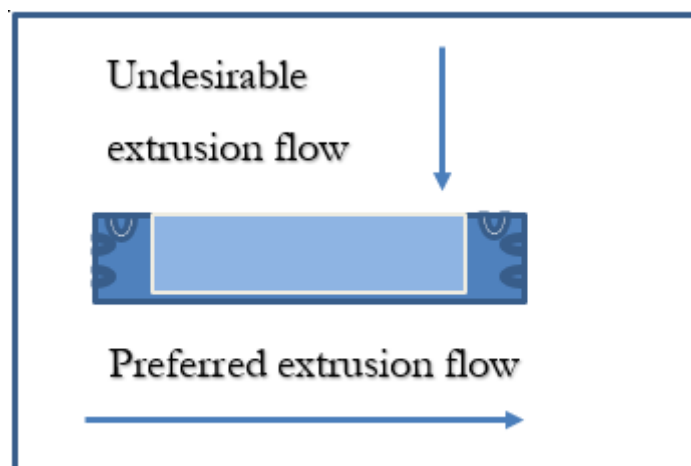


**Figure 5** Schematic of acrylic base showing preferred direction of extrusion.

## 1.2 Aim

The aim of this study is to quantify the diffusion and variability of diffusion of  $^{222}\text{Rn}$  from the acrylic containers used by eriss for gamma spectrometry analysis. The study enables the significance of any  $^{222}\text{Rn}$  leakage on the accuracy and precision of  $^{226}\text{Ra}$  gamma spectrometry measurements to be determined.

## 2 Experimental methods

### 2.1 Samples

Since October 2015 no samples have been prepared for gamma spectrometry analysis in the larger R geometry, only 11 samples have been prepared exclusively for the smaller B geometry and the remaining 554 samples were all pressed in the medium Q geometry. Therefore, all testing was done on samples pressed in ‘Q’ containers.

Three samples containing BL-5 uranium ore reference material mixed with low activity sand were tested for  $^{222}\text{Rn}$  leakage/diffusion using custom-made test chambers (section 2.2) connected to RAD7 radon detectors (sections 2.3). These samples were also used to explore a novel method of identifying potentially leaky containers based on high purity germanium (HPGe) gamma spectrometry counting (section 2.4). Details of the samples are given in Table 1. The samples are calibration standards routinely used for determining the efficiency of the eriss HPGe gamma detectors. All samples had relatively high  $^{226}\text{Ra}$  activity (>400 Bq) and were chosen to minimise counting uncertainties associated with their testing. The samples were prepared (pressed and sealed) in their acrylic container at least 1 month prior to testing to allow for secular equilibrium between  $^{222}\text{Rn}$  and  $^{226}\text{Ra}$ .

Table 1. Samples tested for  $^{222}\text{Rn}$  leakage using test chambers connected to RAD7 radon detectors.

Sample ID	Matrix	$^{226}\text{Ra}$ activity (Bq)
ZQ081	BL-5 mixed with sand	428.9
ZQ083	BL-5 mixed with sand	473.6
ZQ084	BL-5 mixed with sand	498.4

Three additional samples were tested using the test chambers and RAD7 detectors to determine the proportion of ‘free’  $^{222}\text{Rn}$  in the acrylic container (i.e.  $^{222}\text{Rn}$  that has emanated from the sample material and is potentially free to escape the container if not properly sealed). Details of the samples are given in Table 2. The samples included one additional calibration standard and two environmental samples representing typical sediment and biota matrices. They were first tested with the acrylic container lid closed (after allowing sufficient time after pressing and sealing for secular equilibrium between  $^{226}\text{Ra}$  and  $^{222}\text{Rn}$  to establish) and then again with the acrylic container lid open. The former measurements provided additional estimates of  $^{222}\text{Rn}$  diffusion from properly prepared samples, while the latter measurements enabled estimates of free  $^{222}\text{Rn}$ .

Table 2. Samples tested for free  $^{222}\text{Rn}$  using test chambers connected to RAD7 radon detectors.

Sample ID	Matrix	$^{226}\text{Ra}$ activity (Bq)
ZQ082	BL-5 and $^{232}\text{Th}$ mixed with sand	529.5
ZQ012	Sediment	314.2
BQ008	Mussel flesh	2.66

Three waste rock samples from the Ranger trial landform were also tested for free  $^{222}\text{Rn}$  but by an alternate method using HPGe gamma detectors (section 2.4). Sample details are given in Table 3.

Table 3. Samples tested for free  $^{222}\text{Rn}$  using HPGe gamma detectors.

Sample ID	Matrix	$^{226}\text{Ra}$ activity (Bq)
JQ2152	Waste rock	3.88
JQ2153	Waste rock	4.31
JQ2154	Waste rock	5.55

## 2.2 Test chambers

Three custom-made test chambers were manufactured from glued heavy duty PVC pipe fittings, the lid was sealed with a lubricated o-ring and fitted with two tubes for entry and exit of air, with an in-line ball valve in each tube (Figure 6). The test chamber internal dimensions were 100 mm diameter by 70 mm height. The volume was  $\sim 550\text{ cm}^3$ .



Figure 6 Test chamber base, lid with o-ring and inlet and outlet ports, with flexible oil filter wrench to assist in sealing the chamber.

The tubing and test chamber setup were tested for hermetic seal by submerging the equipment under water and increasing the internal pressure to approximately 28,000 Pa with nitrogen gas. No bubbles were observed, indicating that the test chambers and tubing system was air-tight at that pressure.

## 2.3 RAD7 radon detectors

Three DurrIDGE RAD7 radon detectors (<https://durrIDGE.com/products/rad7-radon-detector/>) were used in conjunction with the test chambers to measure  $^{222}\text{Rn}$  diffusion from the acrylic containers. One RAD7 was connected to each test chamber by plastic hoses that attached to the air inlets in the lid of the chamber. An inline air filter (Gelman 0.45  $\mu\text{m}$ ) to avoid particulate contamination of the RAD7 and a drying tube containing a moisture reducing agent completed each setup (Figure 7). The desiccants in the tube were

either silica gel ( $\text{SiO}_2$ , <https://www.silicagel.com.au/1-kg-blue-silica-gel-beads-self-indicating/>) or 8 mesh Drierite ( $\text{CaSO}_4$ , <https://secure.drierite.com/catalog3/page4b.cfm?activeMenu=0>), both of which are neutral to either trapping or emanating  $^{222}\text{Rn}$ .

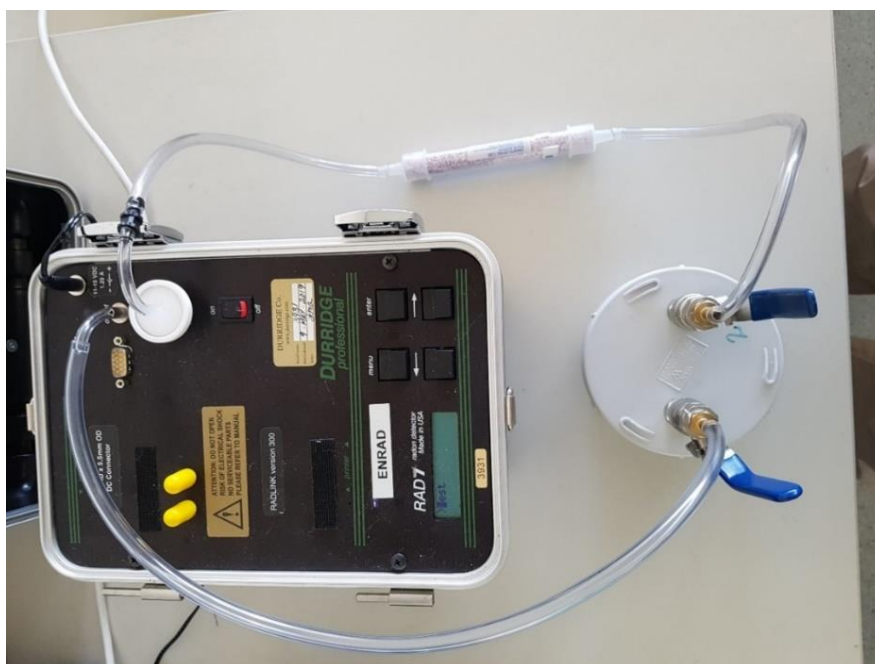


**Figure 7** A complete setup: RAD7, inline filter, plastic tubing, moisture reducer and test chamber.

Each sample in its acrylic container was placed inside the test chamber and the lid of the chamber closed. The build-up of  $^{222}\text{Rn}$  activity concentration inside the chamber due to  $^{222}\text{Rn}$  diffusion from the container was then measured with the RAD7. The RAD7s were operated in NORMAL mode (DurrIDGE 2021) with 1 hour cycle times over measurement periods of 20–30 hours. The data collected and stored on the RAD7s were transferred to a computer via an RS-232/USB cable using the DurrIDGE ‘Capture’ program. The program also applied a humidity correction to the data.

One RAD7 (serial number 3931) was calibrated at DurrIDGE USA prior to commencing the study. The other two units (serial numbers 2527 and 3925) were cross calibrated to it. Cross-calibration plots are included in Appendix A. Instrument backgrounds were regularly checked. All tests were conducted either after a background run using ambient air or after a delay of more than 1 hour from the previous sample test.

The effective volume of the setup was  $\sim 1350 \text{ cm}^3$  and included the volume of the test chamber ( $\sim 550 \text{ cm}^3$ ) and volume of the RAD7 detector chamber ( $\sim 800 \text{ cm}^3$ ). The volume of the hosing connecting the RAD7 to the test chamber of  $28 \text{ cm}^3$  (6 mm diameter  $\times$  1000 mm length) and the estimated 20% interstitial space within the dry tube of  $5 \text{ cm}^3$  (15 mm diameter  $\times$  150 mm length) was compensated for by the volume of the Q container inside the test chamber.

## 2.4 HPGe gamma detectors

Eriss currently uses three Ortec manufactured HPGe gamma detectors for radionuclide analysis of environmental samples. Counting is controlled by Ortec ‘Maestro’ version 7.0 software (<https://www.ortec-online.com/products/application-software/maestro-mca>). Spectrum analysis is performed using ‘FitzPeaks’ version 3.86 software

(<http://www.jimfitz.co.uk/fitzpeak.htm>), following protocols defined in the eriss standard operating procedure for ‘Gamma Analysis using FitzPeaks’.

The HPGe gamma detectors were used to determine the proportion of free  $^{222}\text{Rn}$  in the three waste rock samples detailed in Table 3. The samples were counted for  $^{222}\text{Rn}$  progeny radionuclides ( $^{214}\text{Bi}$  and  $^{214}\text{Pb}$ ) immediately after they were prepared (pressed and sealed) in their acrylic containers and at regular intervals up until secular equilibrium was established.

The HPGe gamma detectors were also used to assess the variation in intensity of the gamma emissions from  $^{214}\text{Bi}$  at 609 keV and  $^{214}\text{Pb}$  at 295.2 and 352 keV relative to the gamma emission from  $^{226}\text{Ra}$  at 186.2 keV for the three samples of BL-5 uranium ore mixed with sand (Table 1). To negate differences in detector calibration, the net counts at peaks of interest were used for comparison. The net counts are the total counts of a peak, less the continuum and instrument backgrounds, and are calculated automatically by FitzPeaks.

## 3 Results and discussion

### 3.1 $^{222}\text{Rn}$ leakage

The RAD7 measurement data for the three samples of BL-5 uranium ore reference material (Table 1) are included in Appendix B and plotted in Figure 8. The data for all samples show a build-up in  $^{222}\text{Rn}$  activity concentration inside the test chamber over the measurement period, indicating that some leakage or diffusion of  $^{222}\text{Rn}$  from the acrylic containers was occurring.

Factors influencing the observed build-up of  $^{222}\text{Rn}$  inside the test chamber include the rate of  $^{222}\text{Rn}$  escape from the acrylic container and the radioactive decay of  $^{222}\text{Rn}$  atoms that have escaped from the container into the chamber. Additionally, as  $^{222}\text{Rn}$  activity concentration in the test chamber increases, the  $^{222}\text{Rn}$  concentration gradient between the sample in the acrylic container and the air in the test chamber decreases and can cause the rate of  $^{222}\text{Rn}$  escape from the container to decrease over the measurement period. The influence of changing concentration gradient can be effectively mitigated by basing the data analysis on measurements made earlier in the period which are less affected by this factor. We have used only the first ten measurements in our analysis of the data.

The model that was used to interpret the build-up in  $^{222}\text{Rn}$  activity concentration in the test chamber over the first ten measurements is:

$$C = \frac{R}{\lambda V} (1 - e^{-\lambda t}) \quad (\text{Equation 1})$$

where:

- $C$  ( $\text{Bq}/\text{m}^3$ ) is the measured  $^{222}\text{Rn}$  activity concentration;
- $R$  ( $\text{Bq}/\text{s}$ ) is the rate of  $^{222}\text{Rn}$  diffusion from the acrylic container;
- $\lambda$  ( $1/\text{s}$ ) is the  $^{222}\text{Rn}$  decay constant;
- $V$  ( $\text{m}^3$ ) is the effective volume of the test system; and
- $t$  ( $\text{s}$ ) is time.

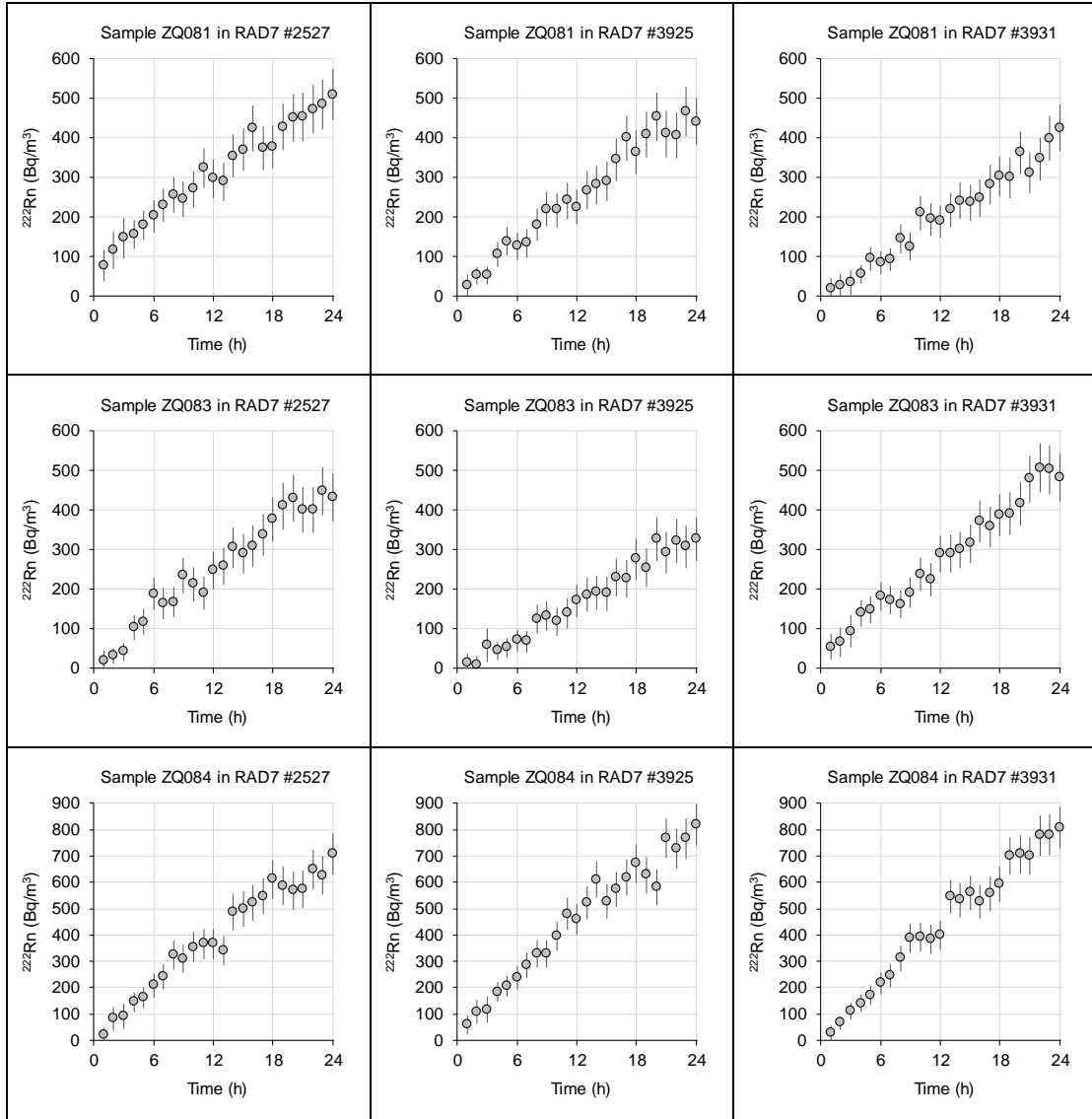


**Figure 8** Build-up of  $^{222}\text{Rn}$  activity concentration inside test chambers.

This model is the solution of the first order differential equation describing the net rate of change in the number of  $^{222}\text{Rn}$  atoms in the test chamber due to escape from the acrylic container and radioactive decay. It assumes that the activity concentration of  $^{222}\text{Rn}$  in the chamber at  $t=0$  is negligible. All parameters in this equation other than  $C$  and  $t$  are constants such that a graph of  $C$  versus  $e^{-\lambda t}$  plotted from the RAD7 measurement data (first ten measurements) should give a linear relationship. The value of  $R$  can be determined from the slope ( $m$ ) of the line of best fit as  $R = -m\lambda V$  or from the intercept ( $b$ ) of the line of best fit as  $R = b\lambda V$ . Figure 9 shows graphs of  $C$  versus  $e^{-\lambda t}$ . The line of best fit and its equation are also shown in the graphs.

Table 4 gives the rate of  $^{222}\text{Rn}$  diffusion ( $R$ ) calculated from the slope and intercept of the line of best fit for each test. The average percentage diffusion of  $^{222}\text{Rn}$  from the containers is given in Table 5. The percentage diffusion was determined by comparing the  $^{222}\text{Rn}$  diffusion rate expressed in atoms per second (i.e.  $R/\lambda$ ) to the sample  $^{226}\text{Ra}$  activity in Becquerels (Table 1). As  $^{226}\text{Ra}$  decays directly to  $^{222}\text{Rn}$ , the sample  $^{226}\text{Ra}$  activity is a measure of the number of  $^{222}\text{Rn}$  atoms produced each second in the sample material.

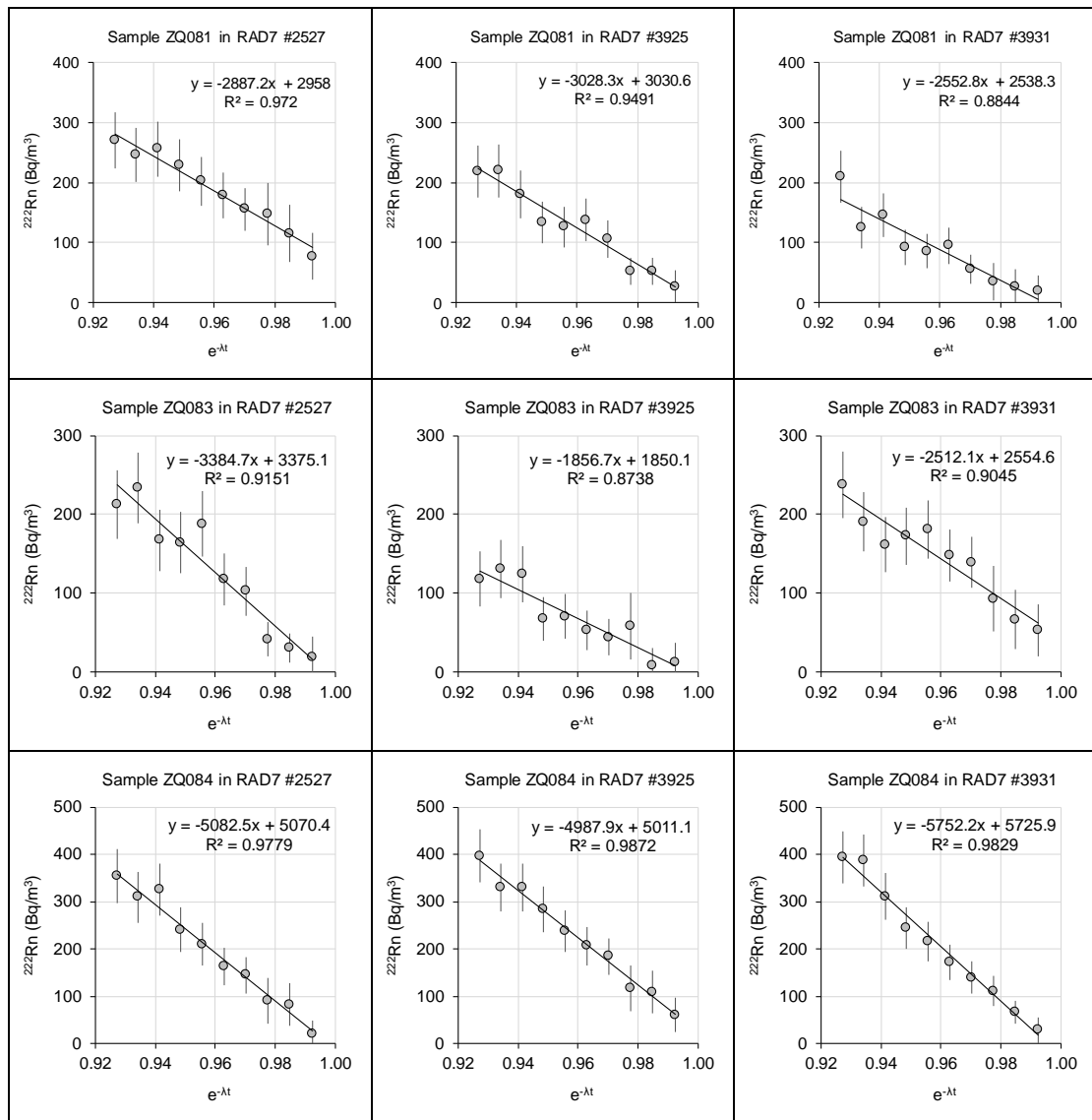


**Figure 9**  $^{222}\text{Rn}$  activity concentration (first ten measurements) versus  $e^{-\lambda t}$  showing lines of best fit.

**Table 4** Rates of  $^{222}\text{Rn}$  leakage from acrylic containers determined from regression fits in Figure 9.

Description	$^{222}\text{Rn}$ diffusion rate from slope	$^{222}\text{Rn}$ diffusion rate from intercept
	( $\times 10^{-6}$ Bq/s)	( $\times 10^{-6}$ Bq/s)
ZQ081 in RAD7 #2527	8.2	8.4
ZQ081 in RAD7 #3925	8.6	8.6
ZQ081 in RAD7 #3931	7.2	7.2
ZQ083 in RAD7 #2527	9.6	9.6
ZQ083 in RAD7 #3925	5.3	5.2
ZQ083 in RAD7 #3931	7.1	7.2
ZQ084 in RAD7 #2527	14.4	14.4
ZQ084 in RAD7 #3925	14.1	14.2
ZQ084 in RAD7 #3931	16.3	16.2



**Table 5**  $^{222}\text{Rn}$  diffusion from acrylic containers as a percentage of total  $^{222}\text{Rn}$  in the sample (mean  $\pm$  standard deviation as determined from diffusion rates in Table 4).

Sample	$^{222}\text{Rn}$ leakage (%)
ZQ081	$0.89 \pm 0.07$
ZQ083	$0.74 \pm 0.20$
ZQ084	$1.4 \pm 0.1$

The average  $^{222}\text{Rn}$  diffusion from each sample container was low at 0.74–1.43% (Table 5). By comparison, gamma spectrometry counting uncertainty for  $^{226}\text{Ra}$ , based on the counting of  $^{222}\text{Rn}$  progeny radionuclides  $^{214}\text{Bi}$  and  $^{214}\text{Pb}$ , is typically 2.5% for most environmental samples analysed by eriss. The results suggest that  $^{222}\text{Rn}$  diffusion from properly prepared samples is unlikely to be a large source of additional uncertainty on  $^{226}\text{Ra}$  gamma spectrometry measurements reported by eriss.

### 3.2 Free $^{222}\text{Rn}$

The RAD7 measurement data for the samples tested for free  $^{222}\text{Rn}$  (Table 2) are included in Appendix B and plotted in Figure 10. Plots of  $C$  versus  $e^{-\lambda t}$  (Equation 1) based on the first ten measurements are shown in Figure 11. The  $^{222}\text{Rn}$  activity concentration for the closed container measurements on mussel flesh sample BQ008 are low (similar to normal  $^{222}\text{Rn}$  in air concentrations), have high uncertainty and do not show a distinct build-up over the measurement period. This is likely due to the low  $^{226}\text{Ra}$  activity (2.66 Bq) of the sample combined with low rate of  $^{222}\text{Rn}$  escape. The data analysis results for this sample may not be reliable.

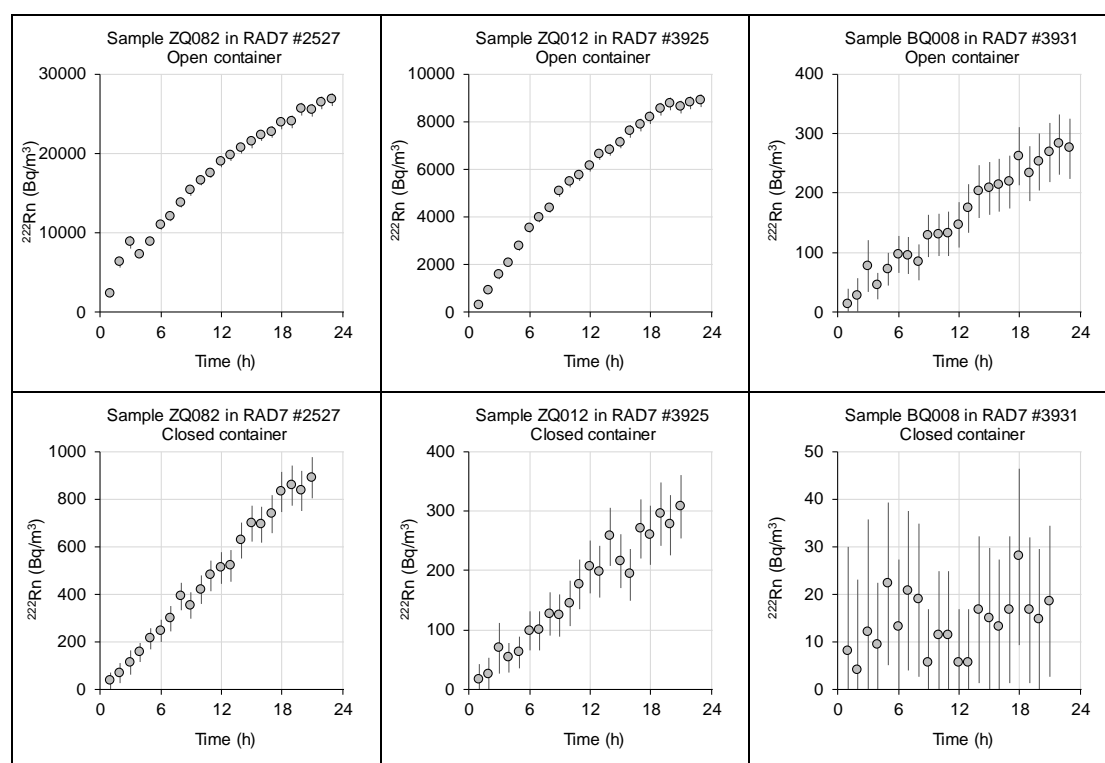


**Figure 10** Build-up of  $^{222}\text{Rn}$  activity concentration inside test chambers from open (top row) and closed (bottom row) acrylic containers.

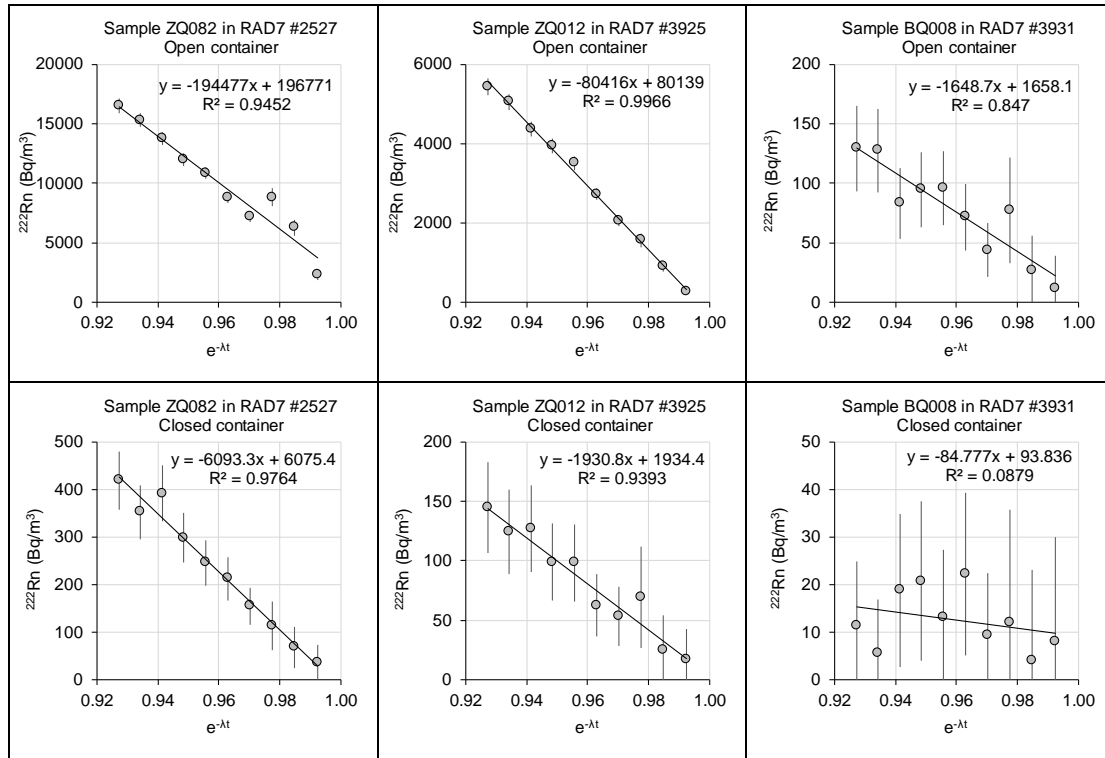


**Figure 11**  $^{222}\text{Rn}$  activity concentration (first ten measurements) versus  $e^{-\lambda t}$  showing lines of best fit to the data for open (top row) and closed (bottom row) acrylic containers.

Table 6 gives the rate of  $^{222}\text{Rn}$  escape calculated from the slope and intercept of the line of best fit to the C versus  $e^{-\lambda t}$  plots (Figure 11). It also gives the average  $^{222}\text{Rn}$  escape from the open and closed sample containers. The results for the open containers give the estimates of the percentage of free  $^{222}\text{Rn}$  relative to total  $^{222}\text{Rn}$  in the sample and provide an upper bound on possible  $^{222}\text{Rn}$  escape from the containers for different sample matrices. More than 33% of the total  $^{222}\text{Rn}$  in these samples is free, with potential to escape from poorly sealed containers. The percentage of free  $^{222}\text{Rn}$  is particularly high for the mussel flesh sample (BQ008) at about 80% and is perhaps related to the non-crystalline sample matrix from which  $^{222}\text{Rn}$  may more easily emanate. These results highlight that if acrylic containers are not properly sealed then there is potential for large uncertainties (i.e. underestimates) in  $^{226}\text{Ra}$  determination by gamma spectrometry based on the counting of  $^{222}\text{Rn}$  progeny radionuclides.

**Table 6** Rates of  $^{222}\text{Rn}$  escape from closed and open acrylic containers determined from regression fits in Figure 11.

Description	$^{222}\text{Rn}$ escape rate from slope ( $\times 10^{-6}$ Bq/s)	$^{222}\text{Rn}$ escape rate from intercept ( $\times 10^{-6}$ Bq/s)	$^{222}\text{Rn}$ escape (%)
ZQ082 in RAD7 #2527 open container	551	558	47
ZQ012 in RAD7 #3925 open container	228	227	33
BQ008 in RAD7 #3931 open container	4.7	4.7	80
ZQ082 in RAD7 #2527 closed container	17.3	17.2	1.5
ZQ012 in RAD7 #3925 closed container	5.5	5.5	0.80
BQ008 in RAD7 #3931 closed container	0.24	0.27	4.0 <sup>a</sup>

<sup>a</sup>Result considered unreliable due to large measurement uncertainties.

The results in Table 6 for the closed container measurements provide additional estimates of  $^{222}\text{Rn}$  diffusion from normally prepared samples. The  $^{222}\text{Rn}$  diffusion estimates for samples ZQ082 and ZQ012 are generally consistent with those obtained for the three BL-5 uranium ore samples (Table 5) and confirm that  $^{222}\text{Rn}$  escape is low from samples that have been prepared in accordance with the standard operating procedure. The closed container results for sample BQ008 are not considered reliable due to high measurement uncertainties (Figure 10).

Table 7 gives the results for the three waste rock samples tested for free  $^{222}\text{Rn}$  by repeated HPGe gamma spectrometry measurements. The ingrowth of  $^{222}\text{Rn}$  in the sample acrylic containers can be seen in the count rate data for the 352 keV gamma emission of  $^{214}\text{Pb}$ . The count rate increases from the first measurement starting on the day of sample preparation until about 2–4 weeks later when secular equilibrium between  $^{222}\text{Rn}$  and  $^{226}\text{Ra}$  is reached. Count rate data for the 338 keV gamma emission of actinium-228 ( $^{228}\text{Ac}$ ) (a member of the thorium-232 decay chain with no connection to  $^{222}\text{Rn}$ ) is also included in Table 7 for reference to show that typical counting variations in this energy region of the gamma spectrum are small (relative standard deviation <5%) and have essentially no bearing on the measured increase in the  $^{214}\text{Pb}$  count rate.

**Table 7** Ingrowth of  $^{222}\text{Rn}$  as measured by the 352 keV emission line of  $^{214}\text{Pb}$ . The data for the 338 keV emission line of  $^{228}\text{Ac}$  is shown for reference and gives typical counting variations for the energy region.

Time <sup>a</sup> (d)	JQ2152V		JQ2153W		JQ2154Y	
	$^{214}\text{Pb}@352\text{ keV}$ (counts/ks)	$^{228}\text{Ac}@338\text{ keV}$ (counts/ks)	$^{214}\text{Pb}@352\text{ keV}$ (counts/ks)	$^{228}\text{Ac}@338\text{ keV}$ (counts/ks)	$^{214}\text{Pb}@352\text{ keV}$ (counts/ks)	$^{228}\text{Ac}@338\text{ keV}$ (counts/ks)
1.3	95.41	13.47	86.45	11.17	140.03	18.51
4.0	105.26	15.23	91.34	12.13	148.53	18.58
7.9	113.19	14.69	91.69	12.15	157.38	19.69
15.2	118.30	14.15	97.49	11.59	163.60	19.17
21.9	119.68	15.08	99.75	12.69	163.78	18.42
28.0	118.14	15.15	92.70	11.43	163.78	19.12

<sup>a</sup> Time that has elapsed from when the sample was pressed to the end of the measurement.

The model used to interpret the increase in the  $^{214}\text{Pb}$  count rate data over the measurement period was:

$$Y = Y_0 + Y_1(1 - e^{-\lambda t}) \quad (\text{Equation 2})$$

where:

- $Y_0$  (counts/s) is the count rate at  $t=0$  when the sample was pressed;
- $Y_1$  (counts/s) is the change in count rate from  $t=0$  to when secular equilibrium is achieved; and
- $\lambda$  (1/s) is the  $^{222}\text{Rn}$  decay constant.

Figure 12 shows the model fitted to the  $^{214}\text{Pb}$  count rate data for each sample. There is strong correspondence between the measurements and model for samples JQ2152V and JQ2154Y but not for sample JQ2153W. The  $^{214}\text{Pb}$  count rate data for sample JQ2153W are variable and do not follow the expected pattern of  $^{222}\text{Rn}$  ingrowth. Results based on the model fit to data for this sample may not be accurate. The source of discrepancy in the measurements has been retrospectively identified as an issue with the specific HPGe detector used to count the sample.

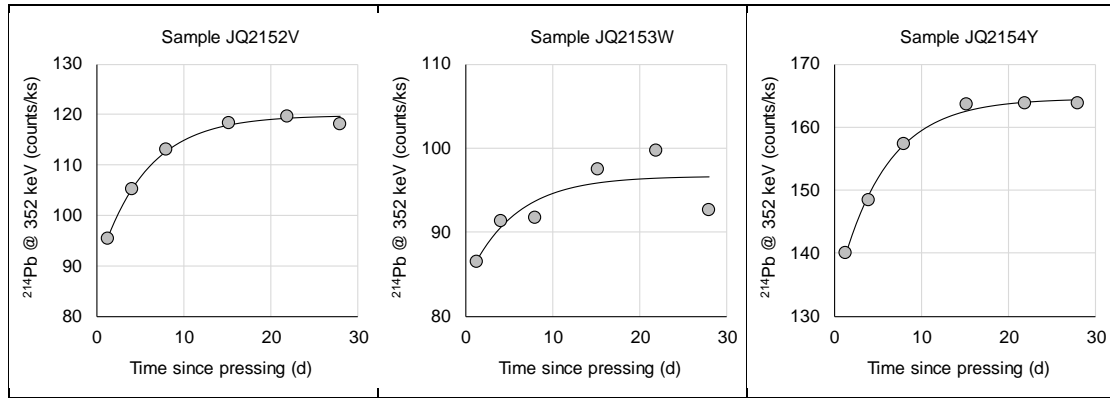


**Figure 12** Model fit to  $^{214}\text{Pb}$  count rate data from repeated sample counts on HPGe gamma detectors.

Table 8 gives the values of coefficients  $Y_0$  and  $Y_1$  determined from non-linear regression analysis using the Minitab 17 statistical software package. Table 8 also gives the proportion of free  $^{222}\text{Rn}$  relative to total  $^{222}\text{Rn}$  in the samples estimated as  $Y_1/(Y_0+Y_1)$ . The results show that up to 25% of the  $^{222}\text{Rn}$  in these samples is free and could potentially escape if the acrylic containers are not properly sealed.

**Table 8.** Coefficients  $Y_0$  and  $Y_1$  determined from fitting Equation 2 to the  $^{214}\text{Pb}$  count rate data and percentage free  $^{222}\text{Rn}$  calculated as  $Y_1/(Y_0+Y_1)$ . Uncertainties in  $Y_0$  and  $Y_1$  are the standard error of the estimate of the model fit.

Sample	$Y_0$ (counts/ks)	$Y_1$ (counts/ks)	Free $^{222}\text{Rn}$ (%)
JQ2152V	$89.6 \pm 1.0$	$30.2 \pm 1.2$	$25.2 \pm 1.3$
JQ2153W <sup>a</sup>	$84.0 \pm 3.2$	$12.6 \pm 4.1$	$13.0 \pm 4.7$
JQ2154Y	$133.4 \pm 0.9$	$31.2 \pm 1.1$	$19.0 \pm 0.8$

<sup>a</sup> Results for this sample are not considered reliable due to anomalies in the measurement data.

### 3.3 Identifying $^{222}\text{Rn}$ leakers

In standards where diffusion is considered to be the only contribution to the loss of  $^{222}\text{Rn}$ , the variation of  $^{222}\text{Rn}$  progeny to  $^{226}\text{Ra}$  parent, as measured by the ratio of peaks areas of the progeny ( $^{214}\text{Bi}$  and  $^{214}\text{Pb}$ ) to  $^{226}\text{Ra}$  at 186.2 keV, was between 1% and 4% (Table 9). The ratios derived from these measurements are independent of the activity and, for the Q geometry, also independent of the matrix (Laxman 2012). The ‘Average Counting Uncertainty’ is the average of the counting uncertainties for each energy emission across all three standards on a detector. All count times were 10,800 seconds.

The ratios of the areas of the emission lines of the  $^{222}\text{Rn}$  progeny to  $^{226}\text{Ra}$  in non-leaking containers are listed in column ‘Ratio:186’. The statistical counting uncertainty, in the ‘Ave. Counting Uncert. %’ column, is dominated by the  $^{226}\text{Ra}$  counting uncertainty. The combined counting uncertainty on each ratio is between 7 to 9% of the ratio. High activity standards give better counting statistics and lower uncertainties, increasing confidence that variations between the ratios would be exposed.

As noted in Section 1.1, the  $^{226}\text{Ra}$  peak at 186.2 keV is overlaid with the 185.7 keV peak of  $^{235}\text{U}$ . The  $^{226}\text{Ra}$  emission at 186.2 keV does not rely on  $^{222}\text{Rn}$  retention, however it is impacted by the contribution of  $^{235}\text{U}$  which is proportional to the uranium content of the sample. Although HPGe detectors have different efficiencies across a range of energies, on any one detector, the ratio of the 186.2 keV emission to the  $^{214}\text{Bi}$  and  $^{214}\text{Pb}$  emissions could be used to assess possible  $^{222}\text{Rn}$  ‘leakers’, despite the variable  $^{235}\text{U}$  contribution at

185.7 keV which could mask possible  $^{222}\text{Rn}$  leakage. This technique is only possible because the energy of emissions (186.2 keV to 609 keV) used in this comparison all have similar linear attenuation characteristics measured over a range of different soil matrices (Laxman, 2012) and the 0.5cm thickness of the samples or standards in Q geometry. The  $^{238}\text{U}$ : $^{226}\text{Ra}$  content can vary between environmental samples and the detector calibration standard, CANMET BL-5, which is in secular equilibrium with progeny radionuclides to  $^{210}\text{Pb}$  ([BL-5 Certificate of Analysis \(nrcan.gc.ca\)](#)).

Applying the above knowledge of the relationship between the activities of the  $^{226}\text{Ra}$  as measured at the 186 keV region and calculated from the  $^{222}\text{Rn}$  progeny ( $^{214}\text{Pb}$  and  $^{214}\text{Bi}$ ) it is possible to identify  $^{222}\text{Rn}$  'leakers' when  $^{226}\text{Ra}$  activity at 186 keV is in excess of  $^{214}\text{Pb}$  and  $^{214}\text{Bi}$  activities. In properly sealed samples, the reverse is always true, i.e.  $^{214}\text{Pb}$  and  $^{214}\text{Bi}$  activities are always in excess of the  $^{226}\text{Ra}$  activity as measured by the 186 keV emission (Figure 13).

The uncertainty provided for  $^{226}\text{Ra}$  in BL-5 documentation is  $\pm 4.4\%$ , which could be a limiting factor in our  $^{226}\text{Ra}$  accuracy. However, we have found that the consistency, or precision, of the  $^{226}\text{Ra}$  in BL-5 standards is closer to  $\pm 2.5\%$  and similar in accuracy, when checked against  $^{226}\text{Ra}$  certified solutions for which the uncertainty is much smaller.

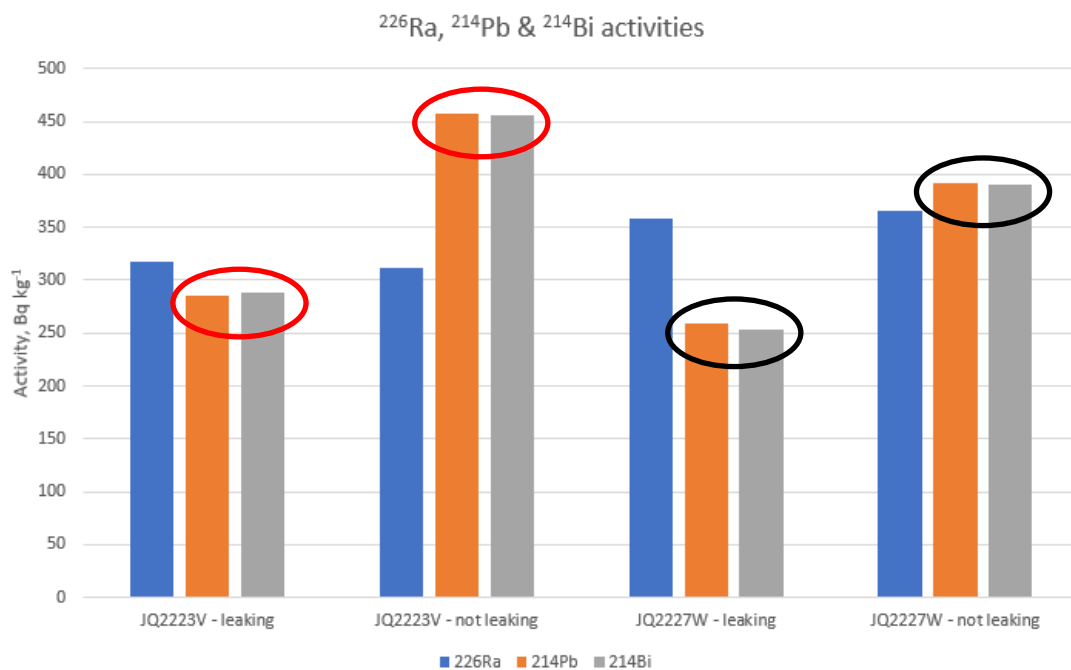


**Figure 13** Activities of  $^{226}\text{Ra}$ ,  $^{214}\text{Pb}$  and  $^{214}\text{Bi}$  in leaking and non-leaking containers for samples JQ2223 and JQ2227 on detectors V and W respectively. The change in activity of  $^{214}\text{Pb}$  and  $^{214}\text{Bi}$  is highlighted.

**Table 9** Ratios of counts for  $^{222}\text{Rn}$  progeny ( $^{214}\text{Bi}$  and  $^{214}\text{Pb}$ ) relative to  $^{226}\text{Ra}$  to illustrate potential ratio variation in non-leaking standards. All count times were 10,800 seconds.

Det - Y	Standard:	ZQ081		ZQ083		ZQ084		Ave. Counting	Ratio :186
Radionuclide	Energy (keV)	Net Counts	Ratio :186	Net Counts	Ratio :186	Net Counts	Ratio :186	Uncert. %	Max % var
$^{226}\text{Ra}$	186	33845		38467		40148		0.8	
$^{214}\text{Pb}$	295	67492	1.994	76845	1.998	78720	1.961	0.3	1.704
$^{214}\text{Pb}$	352	115036	3.399	132413	3.442	137653	3.429	0.3	1.275
$^{214}\text{Bi}$	609	76480	2.260	85417	2.221	89325	2.225	0.4	1.765
Det - W	Standard:	ZQ081		ZQ083		ZQ084		Ave. Counting	Ratio :186
Radionuclide	Energy (keV)	Net Counts	Ratio :186	Net Counts	Ratio :186	Net Counts	Ratio :186	Uncert. %	Max % var
$^{226}\text{Ra}$	186	38979		43191		45913		0.7	
$^{214}\text{Pb}$	295	59905	1.537	65043	1.506	68610	1.494	0.5	2.844
$^{214}\text{Pb}$	352	94066	2.413	103376	2.393	107998	2.352	0.4	2.594
$^{214}\text{Bi}$	609	53146	1.363	57946	1.342	60548	1.319	0.5	3.389
Det - V	Standard:	ZQ081		ZQ083		ZQ084		Ave. Counting	Ratio :186
Radionuclide	Energy (keV)	Net Counts	Ratio :186	Net Counts	Ratio :186	Net Counts	Ratio :186	Uncert. %	Max % var
$^{226}\text{Ra}$	186	48644		50035		56977		0.6	
$^{214}\text{Pb}$	295	80690	1.659	83048	1.660	93181	1.635	0.4	1.491
$^{214}\text{Pb}$	352	129042	2.653	132869	2.656	149614	2.626	0.3	1.129
$^{214}\text{Bi}$	609	73511	1.511	76754	1.534	84900	1.490	0.4	2.948

## 4 Conclusion

The measured rate of  $^{222}\text{Rn}$  diffusion from the eriss gamma spectrometry acrylic containers was generally around 1% of the total  $^{222}\text{Rn}$  (or  $^{226}\text{Ra}$ ) activity in the sample for properly sealed containers. This small amount of  $^{222}\text{Rn}$  loss does not significantly affect gamma spectrometry measurement results for  $^{226}\text{Ra}$  using  $^{222}\text{Rn}$  progeny radionuclides ( $^{214}\text{Bi}$  and  $^{214}\text{Pb}$ ) as proxies for  $^{226}\text{Ra}$ , as gamma spectrometry analysis counting and calibration uncertainties are typically larger than 2%. Also, the rates of  $^{222}\text{Rn}$  diffusion from environmental samples and calibration standards are comparable, further reducing the effect of any  $^{222}\text{Rn}$  diffusion on gamma spectrometry measurements of  $^{226}\text{Ra}$ .

The amount of free  $^{222}\text{Rn}$  inside the acrylic containers can be a considerable proportion of the total  $^{222}\text{Rn}$  (or  $^{226}\text{Ra}$ ) activity in the sample. This free  $^{222}\text{Rn}$  can escape if containers are not correctly sealed and lead to underestimates of  $^{226}\text{Ra}$  activity in environmental samples when measured by gamma spectrometry. The finding emphasizes the need to carefully follow the existing standard operating procedure for gamma spectrometry sample preparation to completely seal the lid, o-ring and base of the acrylic containers, thereby avoiding excessive loss of  $^{222}\text{Rn}$  and inaccurate  $^{226}\text{Ra}$  results.

A poorly-sealed acrylic container will allow a much greater proportion of  $^{222}\text{Rn}$  to escape, or 'leak', from the container and therefore not be counted as progeny. This  $^{222}\text{Rn}$  leakage from samples will result in under reported  $^{226}\text{Ra}$  activity concentrations. A rapid method of identifying poorly-sealed acrylic containers, or 'leakers', is that the activity of  $^{226}\text{Ra}$  at 186 keV is greater than the activity calculated from the  $^{222}\text{Rn}$  progeny emissions ( $^{214}\text{Pb}$  and  $^{214}\text{Bi}$ ). Leaking samples are resealed and recounted, after a delay to reach secular equilibrium, to achieve optimum accuracy and precision of  $^{226}\text{Ra}$  activity concentration.

## References

- Bollhöfer A, Brazier J, Humphrey C, Ryan B & Esparon A 2011. A study of radium bioaccumulation in freshwater mussels, *Velesunio angasi*, in the Magela Creek catchment, Northern Territory, Australia. *Journal of Environmental Radioactivity* 102, 964–974.
- Doering C, McMaster SA & Johansen MP 2018. Modelling the dispersion of radon-222 from a landform covered by low uranium grade waste rock. *Journal of Environmental Radioactivity* 192, 498–504.
- DurrIDGE 2021. RAD7 electronic radon detector user manual. DurrIDGE Company Inc., Billerica. <https://durridge.com/documentation/RAD7%20Manual.pdf>
- IAEA 2010. Worldwide Open Proficiency Test: Determination of Naturally Occurring Radionuclides in Phosphogypsum and Water. IAEA Analytical Quality in Nuclear Applications No. IAEA/AQ/18.
- Laxman C & Dayanand R 2012. Attenuation coefficient of soil samples by gamma ray energy. *Research Journal of Recent Sciences* 1(9), 41–48.
- Leslie C 2009. Analysing environmental radioactivity in soils and sediments using high-purity germanium gamma detectors at CSIRO Land and Water: procedures and protocols. CSIRO Land and Water Science Report 12/09.
- LNHB 2021. Atomic and nuclear data. Laboratoire National Henri Becquerel. <http://www.lnhb.fr/nuclear-data/nuclear-data-table/>
- Marten R 1992. Procedures for routine analysis of naturally occurring radionuclides in environmental samples by gamma-ray spectrometry with HPGe detectors. Internal Report 76, Supervising Scientist.
- Murray AS, Marten R, Johnston A & Martin P 1987. Analysis for naturally occurring radionuclides at environmental concentrations by gamma spectrometry. *Journal of Radioanalytical and Nuclear Chemistry, Articles*, 115(2), 263–288.
- PfITZNER J 1993. Sample collection and preparation manual for gamma-ray spectrometry analysis. Supervising Scientist, unpublished.
- Suursoon S, Kiisk M, Semakalu A & Isakar K 2014. Radon leakage as a source of additional uncertainty in simultaneous determination of  $^{226}\text{Ra}$  and  $^{228}\text{Ra}$  by gamma spectrometry—Validation of analysis procedure. *Applied Radiation and Isotopes* 87, 447–451.



## Appendix A RAD7 cross-calibration plots

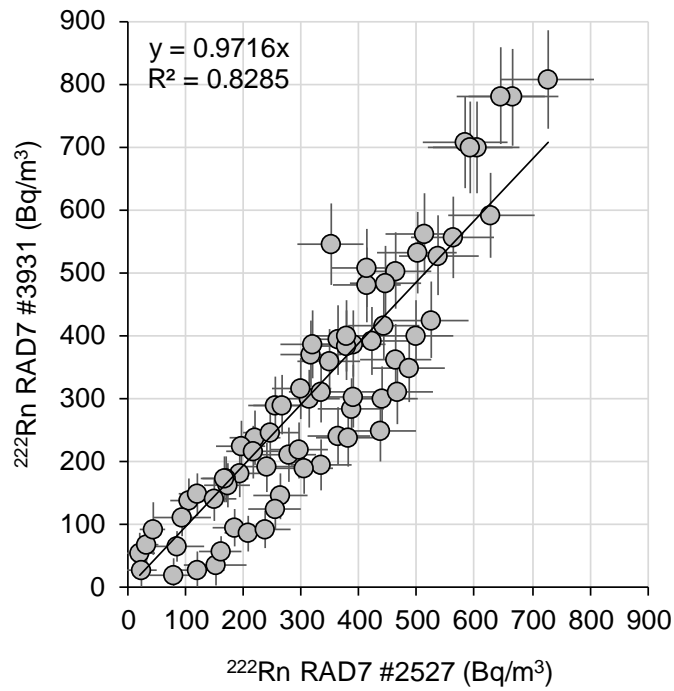


**Figure A1** Cross-calibration of RAD7 #2527 (uncalibrated) with RAD7 #3931 (calibrated).

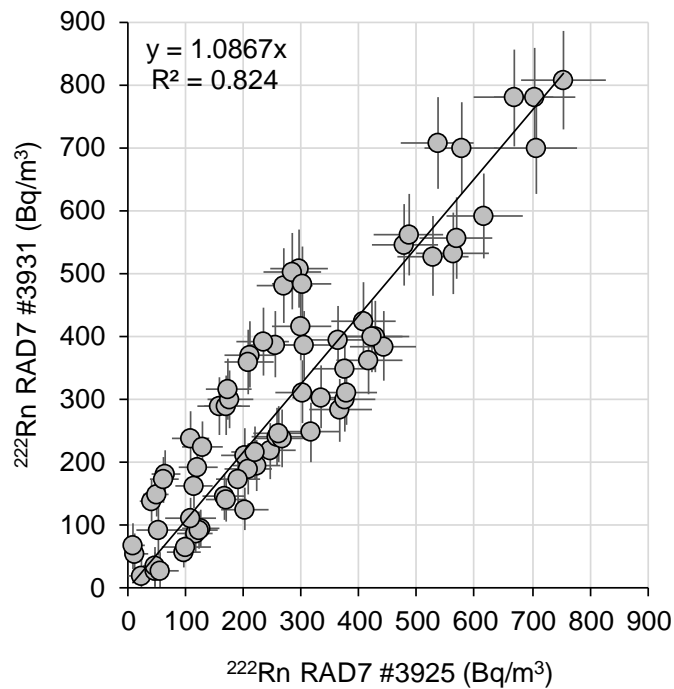


**Figure A2** Cross-calibration of RAD7 #3925 (uncalibrated) with RAD7 #3931 (calibrated).

## Appendix B RAD7 measurement data

**Table B1** RAD7 measurement data from all tests. Data are humidity and calibration corrected. Uncertainty in  $^{222}\text{Rn}$  is 2-sigma of the counts.

Sample	Container	RAD7	Date & time	$^{222}\text{Rn}$ (Bq/m <sup>3</sup> )	$^{222}\text{Rn}$ 2-sigma uncertainty (Bq/m <sup>3</sup> )
ZQ081	Closed	2527	25/11/20 10:02	77	39
ZQ081	Closed	2527	25/11/20 11:02	115	48
ZQ081	Closed	2527	25/11/20 12:02	147	52
ZQ081	Closed	2527	25/11/20 13:02	156	36
ZQ081	Closed	2527	25/11/20 14:02	179	38
ZQ081	Closed	2527	25/11/20 15:02	202	41
ZQ081	Closed	2527	25/11/20 16:02	229	43
ZQ081	Closed	2527	25/11/20 17:02	256	45
ZQ081	Closed	2527	25/11/20 18:02	246	45
ZQ081	Closed	2527	25/11/20 19:02	270	47
ZQ081	Closed	2527	25/11/20 20:02	325	51
ZQ081	Closed	2527	25/11/20 21:02	297	49
ZQ081	Closed	2527	25/11/20 22:02	289	49
ZQ081	Closed	2527	25/11/20 23:02	354	53
ZQ081	Closed	2527	26/11/20 00:02	370	55
ZQ081	Closed	2527	26/11/20 01:02	425	59
ZQ081	Closed	2527	26/11/20 02:02	375	55
ZQ081	Closed	2527	26/11/20 03:02	378	55
ZQ081	Closed	2527	26/11/20 04:02	428	59
ZQ081	Closed	2527	26/11/20 05:02	451	60
ZQ081	Closed	2527	26/11/20 06:02	453	60
ZQ081	Closed	2527	26/11/20 07:02	473	61
ZQ081	Closed	2527	26/11/20 08:02	486	63
ZQ081	Closed	2527	26/11/20 09:02	510	64
ZQ083	Closed	2527	26/11/20 18:08	19	26
ZQ083	Closed	2527	26/11/20 19:08	30	19
ZQ083	Closed	2527	26/11/20 20:08	41	22
ZQ083	Closed	2527	26/11/20 21:08	103	31
ZQ083	Closed	2527	26/11/20 22:08	117	33
ZQ083	Closed	2527	26/11/20 23:08	188	41
ZQ083	Closed	2527	27/11/20 00:08	164	39
ZQ083	Closed	2527	27/11/20 01:08	167	39
ZQ083	Closed	2527	27/11/20 02:08	233	45
ZQ083	Closed	2527	27/11/20 03:08	212	43
ZQ083	Closed	2527	27/11/20 04:08	190	41
ZQ083	Closed	2527	27/11/20 05:08	248	47
ZQ083	Closed	2527	27/11/20 06:08	258	47

Sample	Container	RAD7	Date & time	<sup>222</sup> Rn (Bq/m <sup>3</sup> )	<sup>222</sup> Rn 2-sigma uncertainty (Bq/m <sup>3</sup> )
ZQ083	Closed	2527	27/11/20 07:08	305	51
ZQ083	Closed	2527	27/11/20 08:08	291	50
ZQ083	Closed	2527	27/11/20 09:08	309	52
ZQ083	Closed	2527	27/11/20 10:08	338	54
ZQ083	Closed	2527	27/11/20 11:08	378	56
ZQ083	Closed	2527	27/11/20 12:08	410	59
ZQ083	Closed	2527	27/11/20 13:08	430	60
ZQ083	Closed	2527	27/11/20 14:08	401	58
ZQ083	Closed	2527	27/11/20 15:08	401	59
ZQ083	Closed	2527	27/11/20 16:08	449	61
ZQ083	Closed	2527	27/11/20 17:08	433	60
ZQ083	Closed	2527	27/11/20 18:08	461	62
ZQ083	Closed	2527	27/11/20 19:08	460	62
ZQ083	Closed	2527	27/11/20 20:08	476	63
ZQ083	Closed	2527	27/11/20 21:08	544	67
ZQ084	Closed	2527	22/11/20 13:42	21	28
ZQ084	Closed	2527	22/11/20 14:42	82	46
ZQ084	Closed	2527	22/11/20 15:42	91	48
ZQ084	Closed	2527	22/11/20 16:42	144	38
ZQ084	Closed	2527	22/11/20 17:42	162	40
ZQ084	Closed	2527	22/11/20 18:42	209	45
ZQ084	Closed	2527	22/11/20 19:42	240	48
ZQ084	Closed	2527	22/11/20 20:42	325	55
ZQ084	Closed	2527	22/11/20 21:42	309	54
ZQ084	Closed	2527	22/11/20 22:42	353	57
ZQ084	Closed	2527	22/11/20 23:42	366	58
ZQ084	Closed	2527	23/11/20 00:42	367	58
ZQ084	Closed	2527	23/11/20 01:42	341	56
ZQ084	Closed	2527	23/11/20 02:42	486	67
ZQ084	Closed	2527	23/11/20 03:42	499	67
ZQ084	Closed	2527	23/11/20 04:42	523	68
ZQ084	Closed	2527	23/11/20 05:42	546	70
ZQ084	Closed	2527	23/11/20 06:42	611	73
ZQ084	Closed	2527	23/11/20 07:42	587	73
ZQ084	Closed	2527	23/11/20 08:42	568	71
ZQ084	Closed	2527	23/11/20 09:42	575	72
ZQ084	Closed	2527	23/11/20 10:42	649	76
ZQ084	Closed	2527	23/11/20 11:42	627	75
ZQ084	Closed	2527	23/11/20 12:42	706	79
ZQ081	Closed	3925	26/11/20 18:00	26	28
ZQ081	Closed	3925	26/11/20 19:00	52	23

Sample	Container	RAD7	Date & time	<sup>222</sup> Rn (Bq/m <sup>3</sup> )	<sup>222</sup> Rn 2-sigma uncertainty (Bq/m <sup>3</sup> )
ZQ081	Closed	3925	26/11/20 20:00	52	23
ZQ081	Closed	3925	26/11/20 21:00	105	32
ZQ081	Closed	3925	26/11/20 22:00	138	35
ZQ081	Closed	3925	26/11/20 23:00	126	34
ZQ081	Closed	3925	27/11/20 00:00	133	35
ZQ081	Closed	3925	27/11/20 01:00	180	40
ZQ081	Closed	3925	27/11/20 02:00	220	44
ZQ081	Closed	3925	27/11/20 03:00	218	43
ZQ081	Closed	3925	27/11/20 04:00	242	46
ZQ081	Closed	3925	27/11/20 05:00	225	44
ZQ081	Closed	3925	27/11/20 06:00	267	48
ZQ081	Closed	3925	27/11/20 07:00	281	49
ZQ081	Closed	3925	27/11/20 08:00	290	50
ZQ081	Closed	3925	27/11/20 09:00	346	54
ZQ081	Closed	3925	27/11/20 10:00	400	58
ZQ081	Closed	3925	27/11/20 11:00	363	56
ZQ081	Closed	3925	27/11/20 12:00	407	58
ZQ081	Closed	3925	27/11/20 13:00	454	61
ZQ081	Closed	3925	27/11/20 14:00	410	58
ZQ081	Closed	3925	27/11/20 15:00	407	58
ZQ081	Closed	3925	27/11/20 16:00	467	62
ZQ081	Closed	3925	27/11/20 17:00	442	61
ZQ081	Closed	3925	27/11/20 18:00	434	60
ZQ081	Closed	3925	27/11/20 19:00	493	64
ZQ081	Closed	3925	27/11/20 20:00	506	65
ZQ081	Closed	3925	27/11/20 21:00	533	66
ZQ081	Closed	3925	27/11/20 22:00	544	67
ZQ083	Closed	3925	22/11/20 13:32	12	25
ZQ083	Closed	3925	22/11/20 14:32	8	23
ZQ083	Closed	3925	22/11/20 15:32	58	42
ZQ083	Closed	3925	22/11/20 16:32	44	23
ZQ083	Closed	3925	22/11/20 17:32	52	25
ZQ083	Closed	3925	22/11/20 18:32	70	28
ZQ083	Closed	3925	22/11/20 19:32	68	27
ZQ083	Closed	3925	22/11/20 20:32	124	36
ZQ083	Closed	3925	22/11/20 21:32	131	37
ZQ083	Closed	3925	22/11/20 22:32	118	35
ZQ083	Closed	3925	22/11/20 23:32	139	38
ZQ083	Closed	3925	23/11/20 00:32	171	41
ZQ083	Closed	3925	23/11/20 01:32	185	43
ZQ083	Closed	3925	23/11/20 02:32	192	44

Sample	Container	RAD7	Date & time	<sup>222</sup> Rn (Bq/m <sup>3</sup> )	<sup>222</sup> Rn 2-sigma uncertainty (Bq/m <sup>3</sup> )
ZQ083	Closed	3925	23/11/20 03:32	189	43
ZQ083	Closed	3925	23/11/20 04:32	230	47
ZQ083	Closed	3925	23/11/20 05:32	227	47
ZQ083	Closed	3925	23/11/20 06:32	276	51
ZQ083	Closed	3925	23/11/20 07:32	254	49
ZQ083	Closed	3925	23/11/20 08:32	326	56
ZQ083	Closed	3925	23/11/20 09:32	294	53
ZQ083	Closed	3925	23/11/20 10:32	322	55
ZQ083	Closed	3925	23/11/20 11:32	308	54
ZQ083	Closed	3925	23/11/20 12:32	328	56
ZQ084	Closed	3925	25/11/20 09:55	60	36
ZQ084	Closed	3925	25/11/20 10:55	108	46
ZQ084	Closed	3925	25/11/20 11:55	117	48
ZQ084	Closed	3925	25/11/20 12:55	184	38
ZQ084	Closed	3925	25/11/20 13:55	207	41
ZQ084	Closed	3925	25/11/20 14:55	237	43
ZQ084	Closed	3925	25/11/20 15:55	284	48
ZQ084	Closed	3925	25/11/20 16:55	329	51
ZQ084	Closed	3925	25/11/20 17:55	330	51
ZQ084	Closed	3925	25/11/20 18:55	397	55
ZQ084	Closed	3925	25/11/20 19:55	480	61
ZQ084	Closed	3925	25/11/20 20:55	458	60
ZQ084	Closed	3925	25/11/20 21:55	521	63
ZQ084	Closed	3925	25/11/20 22:55	611	69
ZQ084	Closed	3925	25/11/20 23:55	528	64
ZQ084	Closed	3925	26/11/20 00:55	575	67
ZQ084	Closed	3925	26/11/20 01:55	618	69
ZQ084	Closed	3925	26/11/20 02:55	670	72
ZQ084	Closed	3925	26/11/20 03:55	627	70
ZQ084	Closed	3925	26/11/20 04:55	582	68
ZQ084	Closed	3925	26/11/20 05:55	767	77
ZQ084	Closed	3925	26/11/20 06:55	727	75
ZQ084	Closed	3925	26/11/20 07:55	765	77
ZQ084	Closed	3925	26/11/20 08:55	819	80
ZQ081	Closed	3931	22/11/20 13:25	19	26
ZQ081	Closed	3931	22/11/20 14:25	27	29
ZQ081	Closed	3931	22/11/20 15:25	34	32
ZQ081	Closed	3931	22/11/20 16:25	56	24
ZQ081	Closed	3931	22/11/20 17:25	95	30
ZQ081	Closed	3931	22/11/20 18:25	86	29
ZQ081	Closed	3931	22/11/20 19:25	92	30

Sample	Container	RAD7	Date & time	<sup>222</sup> Rn (Bq/m <sup>3</sup> )	<sup>222</sup> Rn 2-sigma uncertainty (Bq/m <sup>3</sup> )
ZQ081	Closed	3931	22/11/20 20:25	146	36
ZQ081	Closed	3931	22/11/20 21:25	125	34
ZQ081	Closed	3931	22/11/20 22:25	210	43
ZQ081	Closed	3931	22/11/20 23:25	194	41
ZQ081	Closed	3931	23/11/20 00:25	190	41
ZQ081	Closed	3931	23/11/20 01:25	218	44
ZQ081	Closed	3931	23/11/20 02:25	241	46
ZQ081	Closed	3931	23/11/20 03:25	236	46
ZQ081	Closed	3931	23/11/20 04:25	248	47
ZQ081	Closed	3931	23/11/20 05:25	282	49
ZQ081	Closed	3931	23/11/20 06:25	303	51
ZQ081	Closed	3931	23/11/20 07:25	300	51
ZQ081	Closed	3931	23/11/20 08:25	363	55
ZQ081	Closed	3931	23/11/20 09:25	312	52
ZQ081	Closed	3931	23/11/20 10:25	347	54
ZQ081	Closed	3931	23/11/20 11:25	399	58
ZQ081	Closed	3931	23/11/20 12:25	425	60
ZQ083	Closed	3931	25/11/20 09:55	53	33
ZQ083	Closed	3931	25/11/20 10:55	67	37
ZQ083	Closed	3931	25/11/20 11:55	93	41
ZQ083	Closed	3931	25/11/20 12:55	139	33
ZQ083	Closed	3931	25/11/20 13:55	148	33
ZQ083	Closed	3931	25/11/20 14:55	181	37
ZQ083	Closed	3931	25/11/20 15:55	172	36
ZQ083	Closed	3931	25/11/20 16:55	162	35
ZQ083	Closed	3931	25/11/20 17:55	190	38
ZQ083	Closed	3931	25/11/20 18:55	238	42
ZQ083	Closed	3931	25/11/20 19:55	224	41
ZQ083	Closed	3931	25/11/20 20:55	290	46
ZQ083	Closed	3931	25/11/20 21:55	290	46
ZQ083	Closed	3931	25/11/20 22:55	299	47
ZQ083	Closed	3931	25/11/20 23:55	316	48
ZQ083	Closed	3931	26/11/20 00:55	371	52
ZQ083	Closed	3931	26/11/20 01:55	358	51
ZQ083	Closed	3931	26/11/20 02:55	387	54
ZQ083	Closed	3931	26/11/20 03:55	391	54
ZQ083	Closed	3931	26/11/20 04:55	416	55
ZQ083	Closed	3931	26/11/20 05:55	479	59
ZQ083	Closed	3931	26/11/20 06:55	507	61
ZQ083	Closed	3931	26/11/20 07:55	502	61
ZQ083	Closed	3931	26/11/20 08:55	483	60

Sample	Container	RAD7	Date & time	<sup>222</sup> Rn (Bq/m <sup>3</sup> )	<sup>222</sup> Rn 2-sigma uncertainty (Bq/m <sup>3</sup> )
ZQ084	Closed	3931	26/11/20 17:51	28	28
ZQ084	Closed	3931	26/11/20 18:51	66	25
ZQ084	Closed	3931	26/11/20 19:51	111	31
ZQ084	Closed	3931	26/11/20 20:51	140	34
ZQ084	Closed	3931	26/11/20 21:51	172	37
ZQ084	Closed	3931	26/11/20 22:51	216	42
ZQ084	Closed	3931	26/11/20 23:51	245	44
ZQ084	Closed	3931	27/11/20 00:51	311	50
ZQ084	Closed	3931	27/11/20 01:51	386	55
ZQ084	Closed	3931	27/11/20 02:51	393	55
ZQ084	Closed	3931	27/11/20 03:51	384	55
ZQ084	Closed	3931	27/11/20 04:51	400	56
ZQ084	Closed	3931	27/11/20 05:51	546	65
ZQ084	Closed	3931	27/11/20 06:51	532	64
ZQ084	Closed	3931	27/11/20 07:51	561	65
ZQ084	Closed	3931	27/11/20 08:51	527	64
ZQ084	Closed	3931	27/11/20 09:51	556	65
ZQ084	Closed	3931	27/11/20 10:51	592	67
ZQ084	Closed	3931	27/11/20 11:51	700	73
ZQ084	Closed	3931	27/11/20 12:51	707	73
ZQ084	Closed	3931	27/11/20 13:51	700	73
ZQ084	Closed	3931	27/11/20 14:51	779	77
ZQ084	Closed	3931	27/11/20 15:51	781	77
ZQ084	Closed	3931	27/11/20 16:51	807	78
ZQ084	Closed	3931	27/11/20 17:51	960	85
ZQ084	Closed	3931	27/11/20 18:51	926	83
ZQ084	Closed	3931	27/11/20 19:51	941	84
ZQ084	Closed	3931	27/11/20 20:51	897	82
ZQ084	Closed	3931	27/11/20 21:51	1025	88
ZQ082	Closed	2527	10/06/20 13:01	36	36
ZQ082	Closed	2527	10/06/20 14:01	68	43
ZQ082	Closed	2527	10/06/20 15:01	112	51
ZQ082	Closed	2527	10/06/20 16:01	154	39
ZQ082	Closed	2527	10/06/20 17:01	212	45
ZQ082	Closed	2527	10/06/20 18:01	246	47
ZQ082	Closed	2527	10/06/20 19:01	298	52
ZQ082	Closed	2527	10/06/20 20:01	391	59
ZQ082	Closed	2527	10/06/20 21:01	352	56
ZQ082	Closed	2527	10/06/20 22:01	419	61
ZQ082	Closed	2527	10/06/20 23:01	477	65
ZQ082	Closed	2527	11/06/20 00:01	508	67

Sample	Container	RAD7	Date & time	<sup>222</sup> Rn (Bq/m <sup>3</sup> )	<sup>222</sup> Rn 2-sigma uncertainty (Bq/m <sup>3</sup> )
ZQ082	Closed	2527	11/06/20 01:01	518	67
ZQ082	Closed	2527	11/06/20 02:01	626	74
ZQ082	Closed	2527	11/06/20 03:01	697	77
ZQ082	Closed	2527	11/06/20 04:01	693	77
ZQ082	Closed	2527	11/06/20 05:01	737	79
ZQ082	Closed	2527	11/06/20 06:01	829	84
ZQ082	Closed	2527	11/06/20 07:01	858	85
ZQ082	Closed	2527	11/06/20 08:01	834	84
ZQ082	Closed	2527	11/06/20 09:01	890	86
ZQ082	Open	2527	11/06/20 14:54	2262	432
ZQ082	Open	2527	11/06/20 15:54	6283	662
ZQ082	Open	2527	11/06/20 16:54	8798	749
ZQ082	Open	2527	11/06/20 17:54	7171	408
ZQ082	Open	2527	11/06/20 18:54	8774	452
ZQ082	Open	2527	11/06/20 19:54	10874	494
ZQ082	Open	2527	11/06/20 20:54	11987	525
ZQ082	Open	2527	11/06/20 21:54	13752	556
ZQ082	Open	2527	11/06/20 22:54	15279	582
ZQ082	Open	2527	11/06/20 23:54	16534	610
ZQ082	Open	2527	12/06/20 00:54	17508	630
ZQ082	Open	2527	12/06/20 01:54	18844	646
ZQ082	Open	2527	12/06/20 02:54	19763	670
ZQ082	Open	2527	12/06/20 03:54	20622	690
ZQ082	Open	2527	12/06/20 04:54	21389	703
ZQ082	Open	2527	12/06/20 05:54	22236	714
ZQ082	Open	2527	12/06/20 06:54	22666	724
ZQ082	Open	2527	12/06/20 07:54	23799	738
ZQ082	Open	2527	12/06/20 08:54	23961	750
ZQ082	Open	2527	12/06/20 09:54	25565	775
ZQ082	Open	2527	12/06/20 10:54	25446	776
ZQ082	Open	2527	12/06/20 11:54	26406	790
ZQ082	Open	2527	12/06/20 12:54	26796	794
ZQ012	Closed	3925	10/06/20 12:56	16	27
ZQ012	Closed	3925	10/06/20 13:56	24	30
ZQ012	Closed	3925	10/06/20 14:56	69	43
ZQ012	Closed	3925	10/06/20 15:56	53	25
ZQ012	Closed	3925	10/06/20 16:56	62	26
ZQ012	Closed	3925	10/06/20 17:56	98	32
ZQ012	Closed	3925	10/06/20 18:56	99	32
ZQ012	Closed	3925	10/06/20 19:56	127	36
ZQ012	Closed	3925	10/06/20 20:56	124	35



Sample	Container	RAD7	Date & time	<sup>222</sup> Rn (Bq/m <sup>3</sup> )	<sup>222</sup> Rn 2-sigma uncertainty (Bq/m <sup>3</sup> )
ZQ012	Closed	3925	10/06/20 21:56	144	38
ZQ012	Closed	3925	10/06/20 22:56	176	42
ZQ012	Closed	3925	10/06/20 23:56	206	45
ZQ012	Closed	3925	11/06/20 00:56	197	44
ZQ012	Closed	3925	11/06/20 01:56	257	49
ZQ012	Closed	3925	11/06/20 02:56	215	46
ZQ012	Closed	3925	11/06/20 03:56	193	43
ZQ012	Closed	3925	11/06/20 04:56	270	50
ZQ012	Closed	3925	11/06/20 05:56	259	49
ZQ012	Closed	3925	11/06/20 06:56	295	53
ZQ012	Closed	3925	11/06/20 07:56	276	51
ZQ012	Closed	3925	11/06/20 08:56	308	54
ZQ012	Open	3925	11/06/20 14:48	258	75
ZQ012	Open	3925	11/06/20 15:48	904	129
ZQ012	Open	3925	11/06/20 16:48	1558	168
ZQ012	Open	3925	11/06/20 17:48	2038	130
ZQ012	Open	3925	11/06/20 18:48	2729	152
ZQ012	Open	3925	11/06/20 19:48	3511	172
ZQ012	Open	3925	11/06/20 20:48	3944	182
ZQ012	Open	3925	11/06/20 21:48	4363	192
ZQ012	Open	3925	11/06/20 22:48	5054	207
ZQ012	Open	3925	11/06/20 23:48	5440	214
ZQ012	Open	3925	12/06/20 00:48	5728	220
ZQ012	Open	3925	12/06/20 01:48	6129	227
ZQ012	Open	3925	12/06/20 02:48	6609	236
ZQ012	Open	3925	12/06/20 03:48	6809	240
ZQ012	Open	3925	12/06/20 04:48	7107	245
ZQ012	Open	3925	12/06/20 05:48	7591	253
ZQ012	Open	3925	12/06/20 06:48	7861	258
ZQ012	Open	3925	12/06/20 07:48	8155	262
ZQ012	Open	3925	12/06/20 08:48	8516	268
ZQ012	Open	3925	12/06/20 09:48	8749	274
ZQ012	Open	3925	12/06/20 10:48	8626	272
ZQ012	Open	3925	12/06/20 11:48	8792	275
ZQ012	Open	3925	12/06/20 12:48	8887	275
BQ008	Closed	3931	10/06/20 12:59	8	22
BQ008	Closed	3931	10/06/20 13:59	4	19
BQ008	Closed	3931	10/06/20 14:59	12	24
BQ008	Closed	3931	10/06/20 15:59	9	13
BQ008	Closed	3931	10/06/20 16:59	22	17
BQ008	Closed	3931	10/06/20 17:59	13	14

Sample	Container	RAD7	Date & time	<sup>222</sup> Rn (Bq/m <sup>3</sup> )	<sup>222</sup> Rn 2-sigma uncertainty (Bq/m <sup>3</sup> )
BQ008	Closed	3931	10/06/20 18:59	21	17
BQ008	Closed	3931	10/06/20 19:59	19	16
BQ008	Closed	3931	10/06/20 20:59	6	11
BQ008	Closed	3931	10/06/20 21:59	11	14
BQ008	Closed	3931	10/06/20 22:59	11	14
BQ008	Closed	3931	10/06/20 23:59	6	11
BQ008	Closed	3931	11/06/20 00:59	6	11
BQ008	Closed	3931	11/06/20 01:59	17	15
BQ008	Closed	3931	11/06/20 02:59	15	15
BQ008	Closed	3931	11/06/20 03:59	13	14
BQ008	Closed	3931	11/06/20 04:59	17	15
BQ008	Closed	3931	11/06/20 05:59	28	19
BQ008	Closed	3931	11/06/20 06:59	17	15
BQ008	Closed	3931	11/06/20 07:59	15	15
BQ008	Closed	3931	11/06/20 08:59	18	16
BQ008	Open	3931	11/06/20 14:48	12	28
BQ008	Open	3931	11/06/20 15:48	27	29
BQ008	Open	3931	11/06/20 16:48	77	44
BQ008	Open	3931	11/06/20 17:48	44	23
BQ008	Open	3931	11/06/20 18:48	72	28
BQ008	Open	3931	11/06/20 19:48	96	31
BQ008	Open	3931	11/06/20 20:48	95	31
BQ008	Open	3931	11/06/20 21:48	83	30
BQ008	Open	3931	11/06/20 22:48	127	35
BQ008	Open	3931	11/06/20 23:48	129	36
BQ008	Open	3931	12/06/20 00:48	131	37
BQ008	Open	3931	12/06/20 01:48	146	38
BQ008	Open	3931	12/06/20 02:48	173	41
BQ008	Open	3931	12/06/20 03:48	203	44
BQ008	Open	3931	12/06/20 04:48	208	44
BQ008	Open	3931	12/06/20 05:48	213	44
BQ008	Open	3931	12/06/20 06:48	218	45
BQ008	Open	3931	12/06/20 07:48	261	49
BQ008	Open	3931	12/06/20 08:48	233	47
BQ008	Open	3931	12/06/20 09:48	253	48
BQ008	Open	3931	12/06/20 10:48	267	50
BQ008	Open	3931	12/06/20 11:48	282	51
BQ008	Open	3931	12/06/20 12:48	275	51